EROSION OF A CONFINED STRATIFIED LAYER BY A VERTICAL JET – DETAILED ASSESSMENT OF A CFD APPROACH AGAINST THE OECD/NEA PSI BENCHMARK

S. Kelm[1], [2]R. Kapulla, [1,3]H.-J. Allelein

[1] Forschungszentrum Jülich GmbH, 52425 Jülich, Germany

[2] Paul Scherrer Institut, 5232 Villigen PSI, Switzerland

[3] RWTH Aachen University, 52080 Aachen, Germany

s.kelm@fz-juelich.de, ralf.kapulla@psi.ch, allelein@lrst.rwth-aachen.de

ABSTRACT

Recently, a blind CFD benchmark exercise was conducted by the OECD/NEA (2013-2014) based on an experiment in the PANDA facility at the Paul Scherrer Institute (PSI) in Switzerland, investigating the turbulent erosion of a stratified helium rich layer in the upper region of the test vessel by means of a vertical air-helium jet impinging from below. In addition to the 'classical' pointwise measurements available for similar experiments conducted in the past, significant additional efforts were spent on the experimental characterization of the underlying flow field and turbulent quantities by means of particle image velocimetry (PIV) for the benchmark. This data is well suited for a detailed assessment of the driving jet flow and its interaction with the stratified layer. Both are essential in order to avoid elimination of different errors, which is possible if validation is performed in a global manner.

Different impacts on the simulation results, in particular on the jet profile and on the mixing progress, are discussed in this paper. A systematic validation is carried out based on measured and derived quantities. It is identified that e.g. the mesh resolution in the jet and mixing zone has only a minor impact, while small changes in turbulence modeling strategy or the chosen model constants, like Sc_t, significantly affect the simulation results.

KEYWORDS

Hydrogen mixing, stratified layer, turbulent jet, CFD validation, PIV

1. INTRODUCTION / BACKGROUND

The severe nuclear accident at the Fukushima Daiichi NPP (Japan, 2011) affirmed the need to investigate and understand hydrogen transport and mixing in the containment and connected buildings in more detail in order to allow for the design and analysis of appropriate counter measures and accident management procedures. Computational Fluid Dynamics (CFD) is intended to be used in the future to simulate the 3D transport and mixing of steam, hydrogen and other non-condensable gases in containment compartments [1]. One main objective of such a simulation is to investigate conditions under which a local accumulation of hydrogen (stratification) is formed and if or how fast such a light gas layer can be dissolved dissipated again by means of the present buoyancy or momentum driven convective flows.

Following the OECD/NEA ISP-47, the formation of a stratified light gas layer as well as its dissolution dissipation has been studied intensively in different projects e.g. in the frame of the joint OECD/NEA-SETH-2 Project (2007-2010) in order to build an experimental database to improve CFD modeling approaches. On this background, a blind CFD benchmark exercise [2] was conducted based on an experiment in the PANDA facility at the PSI in Switzerland [3] by the OECD/NEA. The experiment describes the erosion of a helium rich layer, confined in the upper region of the test vessel, by means of an

off-axis positioned, vertically oriented turbulent air-helium jet (Re~20.000) emerging from below. This test scenario, in particular the anisotropic turbulence generated by a vertical jet flow which is superimposed by buoyancy, challenges the validity of the Boussinesq approximation, adopted in the Reynolds-Averaged Navier Stokes (RANS) equations. Complementary to pointwise measurements of local gas concentration and temperature, for the benchmark test case significant additional efforts were spent on the experimental characterization of the underlying flow field and turbulent quantities measured with particle image velocimetry (PIV).

The experimental transient was simulated by means of the commercial CFD package ANSYS CFX 15.0 [4]. A CFD approach based on the SST turbulence model, which is supposed to be scaled up to application in a reactor containment, was adopted for the blind benchmark phase. It is based on the validation experience gained previously from similar test cases conducted at the Swiss MiniPanda [5] and PANDA facilities [6], the German THAI facility [7] or the French MISTRA facility [8]. As expected, the global erosion progress, quantified by means of the helium concentration histories, was already well predicted in the blind phase by the model. However, a visible deficiency in the prediction of the jet profile, e.g. centerline and radial velocity, was observed when comparing against the PIV measurements [9] and was also reported for similar modeling approaches [2]. This finding motivated a detailed analysis and refined comparison of the final model against the available measurements presented in this paper.

Based on a brief introduction of the experimental test case in chapter 2 and the modeling approach (chapter 3), the systematic validation strategy aimed at an assessment of single modeling aspects is introduced in chapter 4.1. Different impacts on the simulation results, in particular on the jet profile and on the mixing progress, are discussed in chapter 4.2 and 4.3. It is identified that e.g. the mesh resolution in the jet and mixing zone has only a minor impact, while the detailed comparison against the data, in particular the PIV fields, show that small changes in turbulence modeling strategy or the chosen model constants, like Sc_t, significantly affect the predicted transient. A concluding summary is given in chapter 5.

2. EXPERIMENTAL DATABASE

The test was performed as a clear separate effect test, i.e. only one of the PANDA drywells was used and the boundary conditions were simplified to dry, nearly isothermal and isobaric conditions. The vessel used for the experiment has an inner diameter of *4 m* and a height of *8 m* (Figure 1 left). The air-helium mixture forming the jet, with density *1.047 kg/m³* and a nominal tube exit velocity of *~4.7 m/s*, is injected through a tube which is positioned off-axis by *648 mm* with respect to the axis of symmetry of the vessel. The injection tube has a constant nominal inner diameter of d_t = *75.3 mm* and a *180°* bend *2200 mm* below the tube exit. The straight tube past the bend has a length of *~30* d_t which is long enough that possible disturbances introduced by the bend are removed by the turbulence due to the Reynolds number (Re_{inj} ~ 20000) inside the tube. This was confirmed by velocity measurements at the tube exit (see chapter 4.2). Consequently, the velocity profile at the tube exit shows axisymmetric top hat characteristics with boundary layers typical for turbulent pipe flows. During the entire experiment, the pressure was kept constant at about *0.994 bar* absolute by venting of the air-helium mixture from the vessel via a funnel located at the bottom of the vessel, which was connected to a flexible hose and oriented downwards (Figure 1. The injection tube exit is located *2995 mm* above the bottom of the vessel. A PIV system was used to measure 2D velocity fields with an acquisition rate of *5 Hz* in the vicinity of the jet stagnation point at several sequences during the transient. For the calculation of statistical quantities *1024* image pairs were averaged, resulting in an averaging time interval of *204.8 s* (for detailed information refer to [3]).

The PIV camera was mounted in front of the upper vessel window on a translation stage. By vertically inclining the camera, it was possible to record three different fields-of-view (FOVs) to follow the erosion front progression of the helium layer. The three FOVs are depicted as PosA, PosB and PosC in Figure 1 (left). The coordinate system origin to describe the experiment is located at the bottom of the vessel and the light sheet for the PIV recordings coincides with the x-y plane.

A pointwise measurement of the gas concentrations in the facility was performed by means of two mass spectrometers (MS). Gas was continuously sampled at up to *26* positions and sent to the MS systems

through capillaries, having a tip inner diameter of *0.2 mm*. Each of these tubes is equipped with a thermocouple to record the temperature of the gas at the capillary inlet associated.

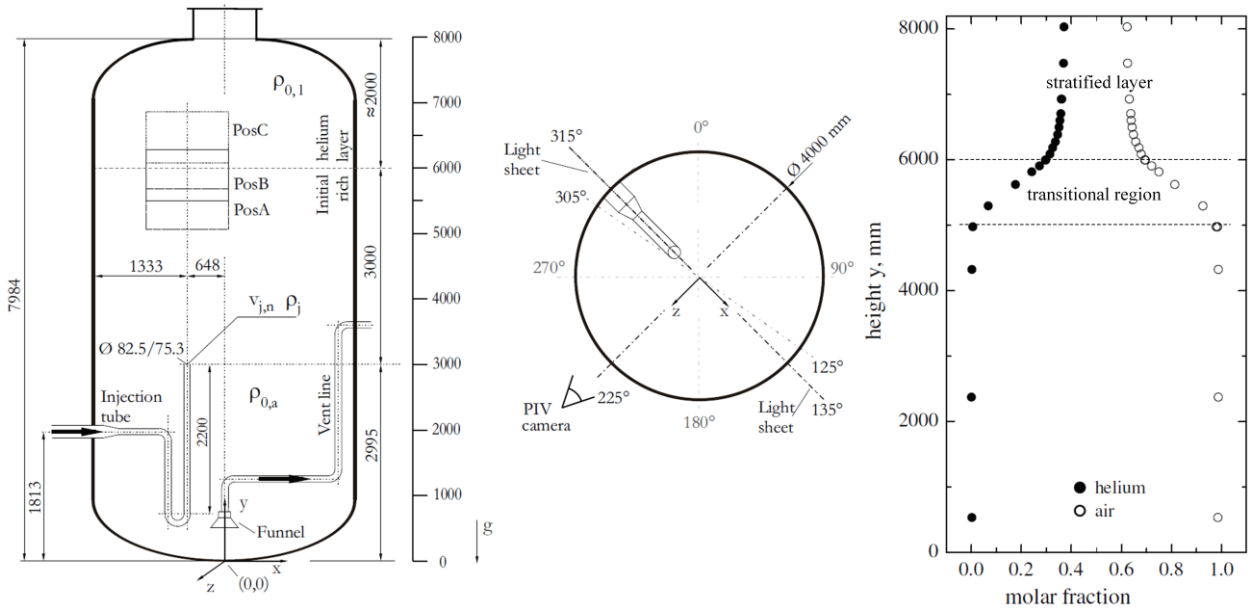

Figure 1: Test setup (left) and initial mixture composition (right) [9]

The MS measurement is sequential and only one line can be selected at a time via a multi-port rotating valve. For the measurement of gas temperatures for the present experiments Type- K thermocouples with a diameter of 1 mm were used. Together with measurements of the vessel wall temperature, a nearly isothermal initial condition of $20°C < T < 22°C$ was confirmed, while the jet temperature increased slightly from $26°C < T_j < 29°C$ during the transient.

Prior to the test, stratified air/helium conditions have been created in the test vessel. A helium-rich air layer with density $\rho_{0,l} = 0.772 kg/m^3$ occupies the region $y > 6000\ mm$, while pure air with density $\rho_{0,a} = 1.173 kg/m^3$ fills the region below $y = 5000\ mm$ (Figure 1 right). In between, there is a transitional region where the helium content increases continuously. The helium molar fraction profile was used as initial condition for the simulation.

A more detailed description of the experiment and measurements can be found in [3]. A comprehensive specification of the test setup and initial and boundary conditions is given in [4].

3. MODELING APPROACH

The fundamental modeling strategy is based on a U-RANS approach which can be directly scaled-up to containment scale without changing the representation of the governing physics in the models. This modeling approach has been applied and validated against several experiments and benchmark cases (e.g. [10], [12]) of containment-typical flow and mixing processes. Even though the results of the benchmark contribution discussed in [9] were blind predictions, they are based on previous validation experience gained on the OECD/NEA SETH-2 tests and similar test cases analyzed in the frame of benchmarks within the German CFD alliance (e.g. THAI-TH26 [7] or MiniPanda [5]). As expected, the global erosion progress, quantified by means of the helium concentration histories, was predicted well by the model (blind results are added as a reference in Figure 6 and Figure 10). However a visible deficiency in the prediction of the jet profile, e.g. centerline and radial velocity, was observed when comparing against the PIV measurements (blind results are added as a reference from Figure 7 to Figure 9).

This finding may indicate an elimination of different model errors and thus a comprehensive and systematic analysis of the impact of different modeling choices on the predicted jet profiles was carried out. This paper

focusses on the validation of the final model, however, characteristic results of the parametric variations are included where appropriate.

3.1 Geometry and Mesh

In order to describe the transport and mixing processes directly at the layer interface and in the multi-compartment domain, the full vessel is considered in the model geometry without additional boundary conditions or symmetries. The main simplifications are related to the internal structures. The vertical part of the air injection line (~20d_h) is resolved by the mesh in order to allow a realistic representation of the jet profile at the pipe exit and its effect on the jet entrainment. The effect of the simplification of the injection line on the jet profiles is discussed in chapter 4.2. All other internals and structures (e.g. measurement and its support, funnel, flanges) are assumed to have only a marginal impact on the mixing progress and are thus neglected in the geometric model and the mesh.

The fluid domain is discretized by means of a block-structured hexahedral mesh (Figure 2) taking into account the common BPGs [13], [14] and [15] as well as code specific recommendations [4].

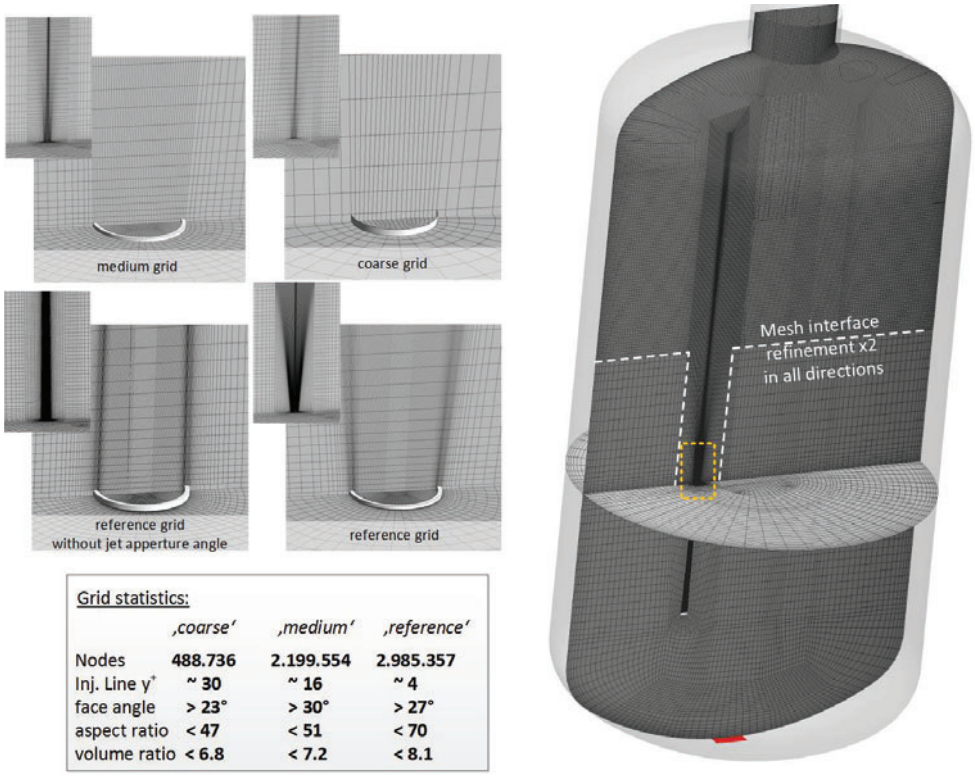

Grid statistics:

	‚coarse'	‚medium'	‚reference'
Nodes	488.736	2.199.554	2.985.357
Inj. Line y^+	~ 30	~ 16	~ 4
face angle	> 23°	> 30°	> 27°
aspect ratio	< 47	< 51	< 70
volume ratio	< 6.8	< 7.2	< 8.1

Figure 2: Reference mesh used of the open analysis and hierarchy of mesh resolutions of the jet flow investigated

The mesh resolution is evenly distributed in the bulk and refined close to the air jet axis and the vessel walls where gradients due to shear layers and the mixing processes are expected. Mesh quality has been optimized in terms of face angle, aspect ratio and volume ratio. The aspect ratio of the cells is small especially above the injection line exit where the significant mixing processes occur. With respect to numerical efficiency, the grid has been coarsened in regions, which are not important for the jet layer interaction, i.e. the volume below the helium cloud except the trajectory of the jet. Grid independency of the U-RANS solution obtained on the medium grid has been demonstrated by means of a grid, coarser by a factor of eight, based on the helium concentration histories already for the blind benchmark submission [9]. Due to the fact that the focus of the open analysis is on the jet profiles, a reference grid with similar bulk resolution, but a significantly refined mesh resolution in the jet was built and also the effect of including a jet aperture angle

in the mesh was investigated. It was identified that the change of the mesh resolution between the medium and reference grid as well as the aperture angle has only a marginal effect on the jet profiles. I.e. differences observed between the open and blind analysis can be related to the remaining model aspects.

3.2 Physical Model and Numerical Settings

In order to describe the gas mixing and transport processes inside the vessel, an unsteady Reynolds Averaged Navier Stokes (U-RANS) approach was chosen. This modeling approach was developed for large scale containment application and intended to be scaled up without change in the fundamental physical models. Based on the previous validation experience, the k-ω based shear stress transport (SST) turbulence model was adopted for the blind prediction. Even though the SST model mainly runs in the k-ε mode, there are visible differences to the standard k-ε model and the measurement (discussed in chapter 4). Consequently, the standard k-ε model was chosen for the final open analysis. Species transport and mixing is considered by an additional transport equation for the helium mass fraction. Heat transport is described by the total energy equation, while radiative heat transfer is neglected due to the minor temperature differences. Buoyancy effects are considered by means of the full density based buoyancy model and production and dissipation terms for turbulence in the k and ω or ε equation. The fluid is assumed to be an ideal mixture which properties are determined according to [16]. The physical CFD model is summarized in Table I.

Table I. Physical CFD model

ANSYS CFX 15	***blind***	***open***
governing equations	U-RANS, total energy equation, transport equation for helium mass fraction	
turbulence model	k-ω based Shear Stress Transport (SST) model	standard k-ε model
	including production and dissipation terms for buoyancy turbulence; Pr_t~0.9, Sc_t~0.9	
equation of state	ideal gas	
buoyancy model	density based	
mixture properties	evaluated according to [16] diffusion coefficient $D_{He/air}$ = 0.72 cm²/s	

The simulation is initialized by means of the specified atmospheric conditions [4] and the experimental vertical helium gradient, while the atmosphere is assumed to be at rest (u,v,w = 0 m/s, k,ω/ε = 1e-20). The transient boundary conditions, i.e. injection temperature are prescribed according to the experimental measurements.

The injection line is simply considered as an adiabatic wall, representing the wall thickness of the pipe. Consequently, the resulting air jet temperature profile in the line is homogeneous in the simulation, while in the experiment, the thermal inertia of the injection line may cause a bend profile. This detail was neglected because the gas temperature differences are low and not considered to have a major effect on the flow. The definition and effect of the turbulent boundary conditions at the injection line inlet are discussed in detail in chapter 4.2. A high turbulence intensity of *I=10%* was identified to be most appropriate for the chosen simplification of the injection line geometry, while for the blind simulation a value of *I=5%* was prescribed. The vessel walls represent the dominant heat sink for the gas and thus the gas to wall heat transfer was resolved by means of a grid refinement close to the wall. The walls are manufactured from steel, i.e. they are characterized by a high heat capacity and thus they were modeled by means of a fixed temperature boundary condition equal to the initial wall temperature. The vent opening is considered by means of a pressure boundary condition (relative pressure *0 Pa*).

The selection of numerical schemes and convergence criteria have been approved according to the BPGs based on a similar case [5]. Basically, the default numerical schemes of CFX 15 are applied. The investigated scenario progresses fairly straight forward and it was identified that the chosen time steps size affects mainly the convergence behavior. Consequently the time step is adjusted in order to achieve good

convergence with only three internal iterations leading to a time step of 0.1s (average CFL number of ~*9*). The time steps are initialized by extrapolation of the previous results due to a better convergence. The high resolution blended scheme is applied; A comparison against a 2nd order scheme didn't reveal differences in the solution during the prior analysis of similar cases. Convergence is monitored by means of the local and integral equation residuals and the global balance errors.

The global helium mass, i.e. sum of inventory and integrated loss at the vent, is conserved with an error of less than 1% of the theoretical mass (sum of initial and injected mass). A very good convergence behavior is observed and for most of the simulation, the dominant convergence criteria is the minimum number of inner coefficient loops (a minimum of three coefficient loops is recommended for buoyant flows by ANSYS [4]). Due to the very good convergence and forced minimum number of three internal iterations per time step, residuals higher that *1e-3* do not occur.

4. OPEN ANALYSIS

4.1 Validation Strategy

The erosion of the stratified layer occurs mainly due to turbulent mass transfer in vicinity of the jet stagnation point. Consequently, the progression of the mixing depends on both the distribution of jet momentum, as well as the turbulence level in the mixing zone. In previous validation cases (e.g. [5]), there was no characterization of the flow available, therefore an implicit validation was performed on basis of local gas concentrations and temperature field measurements.

Turbulent kinetic energy (TKE) is generated and dissipated inside injection line, the shear layer of the free jet and finally at the redirection of the jet flow close to its stagnation point. The resulting turbulent diffusivity at the mixing zone provides the turbulent erosion of the layer. Following this logic, the model validation addresses first the flow inside the injection line by means of a comparison of the jet TKE and vertical velocity profiles at the injection line exit. In order to allow for a further comparison of simulation and PIV data fields it is proved that the global mixing progress, characterized by means of the upward motion of the jet stagnation point is comparable. On this basis, a detailed analysis of the PIV data fields in the vicinity of the stagnation point with focus on the vertical velocity component and the TKE was performed. Once the flow field is predicted consistently with the experimental data, a comparison of the mixture density along the jet axis is performed in order to assess the jet momentum $\rho \cdot \bar{v}$ at the mixing zone. As a last step, the local helium concentrations are compared in order to investigate the turbulent mass transfer and transport from the mixing zone to the vent. The latter step is similar to previous validation runs, while a direct assessment of the flow field is done for the first time on basis of the new experiment.

4.2 Effects on jet profiles

Basically, there is one dominant user decision which affects the jet characteristics at the injection line exit. It is the geometrical representation or simplification of the injection line geometry together with an appropriate definition of the corresponding inlet boundary conditions. The most consistent approach is to resolve the whole injection line according to [4] and to place the inlet boundary outside the vessel (see Figure 3 right). Following this modelling strategy, the resulting velocity profile and turbulence intensity, or turbulent kinetic energy (TKE), at the injection line exit are independent from the inlet definition (e.g. 'block profile') and thus only a result of flow development as well as the TKE production and dissipation inside the feed line.

The predicted radial jet profiles, evaluated right above the injection line exit, are compared to the measurements in Figure 3. The measured jet is quasi axisymmetric, while the simulations show a visible asymmetry resulting from various flow separations at the bends in the feed line. Due to the fact that the injection line is modeled as a smooth tube, local disturbances such as connecting flanges, which homogenize the flow are not considered and may explain the deviation. The velocity magnitudes measured

at the injection characterization tests outside the vessel are lower by approx. 10% compared to the simulation results and may indicate an inconsistency in the specification which needs further clarification. For the sake of comparison, the velocity profiles were normalized by the jet core (i.e. maximum) value. The TKE level in the jet core is well reproduced, while in the shear layer the production is visibly too low.

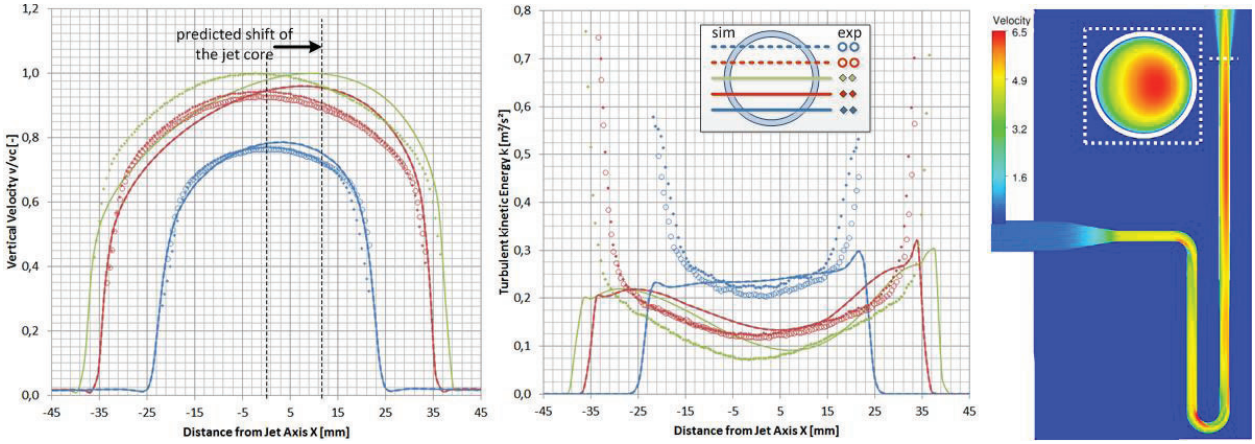

Figure 3: Comparison of radial jet profiles at the injection line exit axial velocity (m), turbulent kinetic energy (middle) and flow visualization (right)

In order to provide an axisymmetric and numerically efficient prediction of the jet, the injection line was simplified to the straight vertical part and the inlet boundary was placed roughly ~20 d_h below the exit level. Appropriate boundary conditions for the turbulent quantities k and ε (or ω) are estimated by the following relations [4]:

$$k = \tfrac{3}{2} I^2 U^2 \quad \text{and} \quad \varepsilon = \frac{k^{3/2}}{0.3 d_h} \tag{1}$$

where I is the turbulence intensity (u'/U) and d_h is the hydraulic diameter of the injection line (*75.3 mm*). According to [4], the default value of the turbulence intensity (*I=5%*) was chosen for the blind simulations [9]. The resulting radial jet profiles compared 6 mm above the tube exit are given in Figure 4.

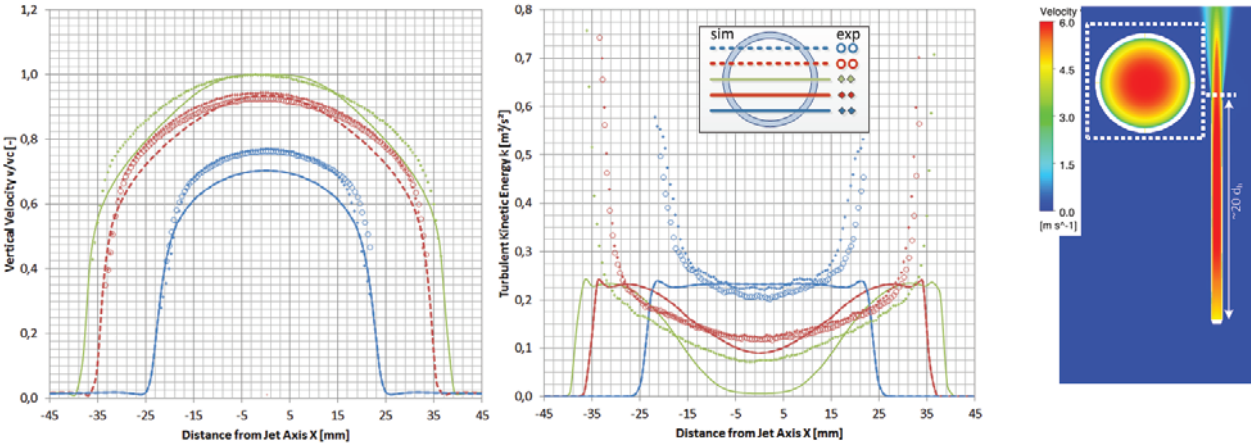

Figure 4: Comparison of radial jet profiles at the injection line exit axial velocity (m), turbulent kinetic energy (middle) and flow visualization (right)

It is obvious that both the normalized jet velocity profile and the turbulent kinetic energy differ significantly both in magnitude and shape from the measured profiles. Considering the centerline (green), one can identify a sharper velocity profile together with an under prediction of the TKE in the jet core. Furthermore, the rapid increase in the shear layer observed in the measurements is not predicted at all.

This deficiency may be either related to TKE production and dissipation within the tube or the definition of the turbulent boundary conditions at the inlet. Consequently, the turbulence intensity I was increased to *10%* resulting in higher values of k and ε (or ω) at the inlet. The corresponding velocity profiles and the jet core TKE level (see Figure 5) are consistent with the measurement, while there is still a deviation in the shear layer.

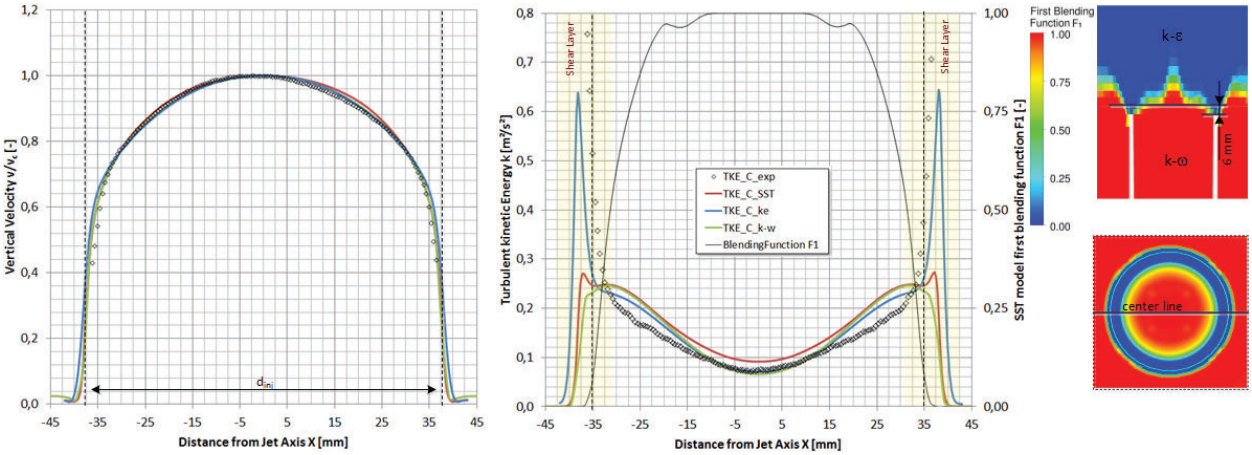

Figure 5: Comparison of radial jet profiles at the injection line exit axial velocity (m), turbulent kinetic energy (middle) and flow visualization (right)

This deviation is related to the automatic blending between the k-ω and k-ε mode in the SST model. Figure 5 illustrates this based on the radial profiles on the centerline by means of the standard kω and kε simulation as well as the bending function F_1 values. It is obvious that the k-ω solution does not provide the TKE in the shear layer, while the k-ε accounts for the rapid increase. Considering that a value of F_1=1 indicates the kω mode, the jet core is simulated by the k-ω model and the shear layer by the k-ε mode (F_1=0). In between there is a smooth blending which explains the nearly complete disappearing of the shear layer TKE in the SST simulation. The SST model provides a k-ω solution within the tube while the free jet and mixing process is modeled in the k-ε mode (see blending function in Figure 5 right).

Generally, the present flow does not require the k-ω capabilities of the SST model, therefore the standard k-ε model was considered for the final analysis in order to avoid further impacts of the blending. Nevertheless, the 'blind' SST model results are included as a reference in the following comparison.

4.3 Transient Analysis

In order to allow for a consistent comparison of the PIV measurements to the CFD results, one has to verify that the transient progression of the scenario is comparable, i.e. the FOV captures a consistent jet position. This requirement is proved by means of a comparison of the erosion front elevation or jet stagnation point position during the test sequence. The stagnation point position on the injection line axis is determined by tracking the elevation of maximum vertical density gradient in the simulation. For the experiment a similar procedure was used, i.e. the density was evaluated for the capillary positions, fitted by a function and used to derive the position of the maximum gradient [9]. A good approximation of the overall erosion front elevation $y[mm]$ as a function of time $t[s]$ in the experiment, considering the given coordinate system is provided through the correlation:

$$y^{-1} = a + b \cdot t^{0.5} \tag{2}$$

where t=time [s], $a = 1.782 \cdot 10^{-4} \left[\frac{1}{m}\right]$ and $b = -7.37 \cdot 10^{-7} \left[\frac{1}{m \cdot \sqrt{s}}\right]$.

Figure 6 illustrates the erosion front progression for the experiment and three simulations, the blind prediction, summarized in [9], the 'final' simulation based on the k-ε model, described before and a simulation using a slightly reduced turbulent Schmidt number of Sc_t = 0.7 (Fluent default value).

The erosion process during the first 800 s is relatively fast (steep slope) since the transitional region of the density gradient poses only a weak resistance to the jet propagation and the jet velocity is higher due to the initial low distance from the injection line exit. Once the transitional region is eroded, the erosion speed (slope of the curve) is reduced and shows a nearly linear characteristic (1500<t<3700s). Beyond this time, only one measurement point at the vessel axis is available (not given in the figure), indicating that the erosion speed is slowed down towards the end of the transient.

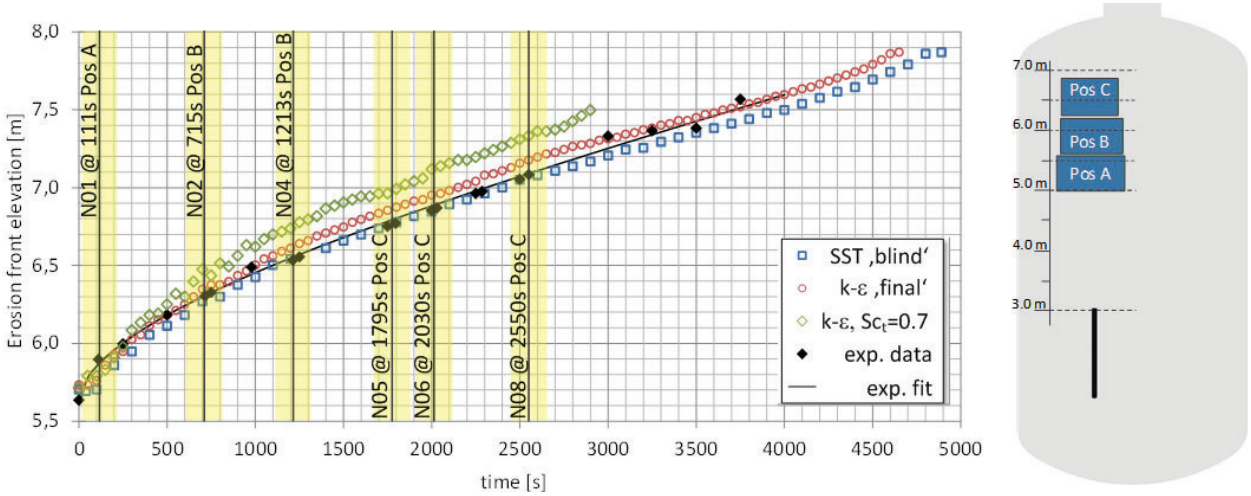

Figure 6: Comparison of measured and simulated erosion front progression. Agreement is mandatory for comparison of PIV data fields

The three simulations clearly show a similar trend, however a further undamped linear progression of the erosion is also observed in the upper dome region (*y>7500 mm*). It is obvious that the case with an increased turbulent diffusion (reduced Sc_t) progresses considerably faster and thus a direct comparison to the PIV data (measurement sequences are depicted in yellow) becomes more and more meaningless with increasing time. The transient evolution of 'blind' and the 'final' simulation are in good agreement with the experiment. As seen later the jet stagnation point position in the 'final' simulation is slightly higher than in the experiment for the PIV sequences N05 to N08. However, the difference is limited and thus the data sets remain comparable.

Based on the good overall agreement of the transient progression, the underlying flow and driving the erosion process can be validated by means of the 2D PIV field data. In order not to lose information, a direct comparison of the averaged 2D fields is performed. In addition to this qualitative assessment, horizontal profiles were extracted and validated. The position of these profiles, indicated in the figures, was chosen according to the benchmark specification [4] in order to allow for a direct comparison. Nevertheless, it is clear that the position is somehow arbitrarily chosen for each sequence and not fixed e.g. with a certain distance to the stagnation point. Along with the vertical component $\bar{v}$ of arithmetic mean velocity, the TKE is also compared. The latter was calculated from the 2D PIV data by assuming axis symmetry of the jet, i.e. the turbulent fluctuations in z-direction (w') are identical to those in x-direction (u'). Thus, the TKE k is quantified by the root mean square of the turbulence normal stresses

$$k = \tfrac{1}{2}\left(2 \cdot \overline{u'u'} + \overline{v'v'}\right) \tag{3}$$

It may be noted that the experimental data shows an anisotropy of the turbulent fluctuations, where the vertical (axial) component is dominant roughly by a factor of two, while the simulations, based on the eddy viscosity concept, assume isentropic turbulence.

The progress obtained in the open evaluation phase (depicted as *k-ε 'open'*) is demonstrated by including the profiles predicted during the blind benchmark phase (depicted as *SST 'blind'*) as a reference. Considering in particular the non-linear progression of the erosion process within the first 800 s, a transient averaging of the simulation results, analogous to the PIV post-processing, is mandatory to account for the motion of the stagnation point during the averaging interval of $\Delta t = 204.8\ s$. In the following figures the bandwidth of results in the averaging interval is indicated by a single standard deviation band.

In the very beginning of the erosion process at *t=111 s* the FOV (PosA) points to the transitional region of the initial density gradient (see Figure 1) which introduces only a weak resistance to the jet. The stagnation point is above the FOV. Below the helium layer, the jet undergoes a slight acceleration due to its buoyancy related to the heavier ambient air. Consequently, this data set allows for the most clear in-vessel validation of the fundamental jet characteristics, i.e. its entrainment and the TKE produced inside the shear layers. The corresponding simulation and experimental results are summarized in Figure 7. Considering the vertical velocity, it is clear that the jet entrainment rate is slightly over predicted, resulting in a velocity decay that is visibly too fast in the jet core and an accordingly broader jet diameter. Nevertheless, considering the horizontal profile evaluated near the lower edge of the FOV where the damping effect of the density gradient is less significant, one can quantify only a minor deviation between 'final' simulation and measurement.

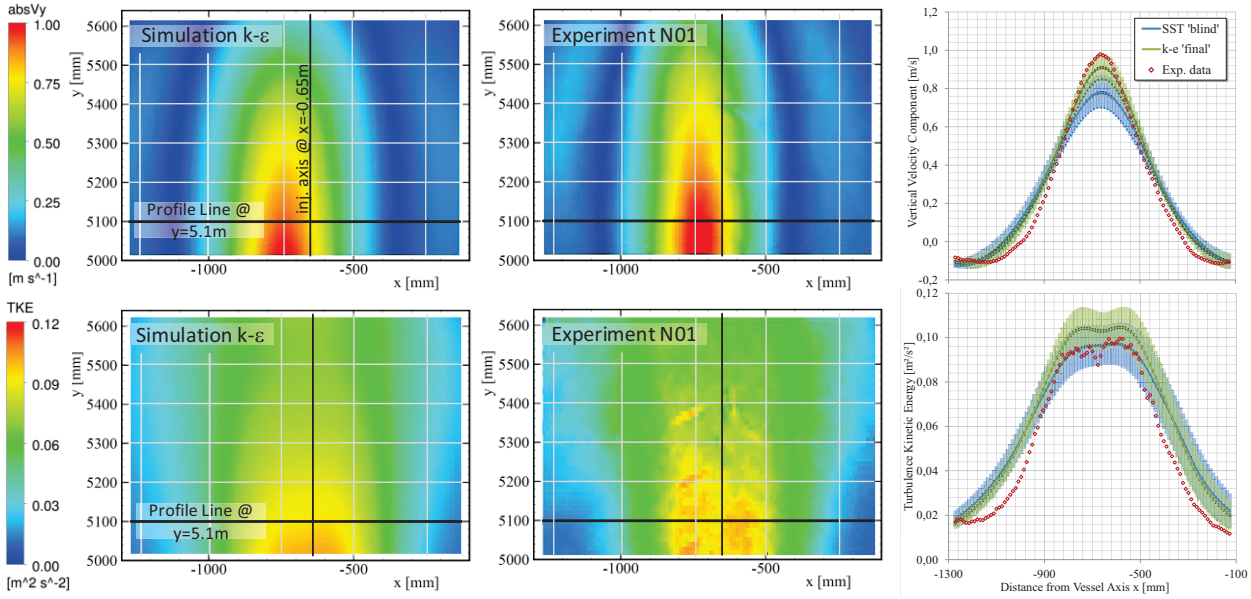

Figure 7: Comparison of averaged fields of the vertical velocity (left) and turbulence kinetic energy (middle) and extracted horizontal profiles (right) at t=111 s (averaging interval: 204s)

The TKE production in the shear layer of the jet was predicted in quite good agreement with the measurement even though the model is based on assumption of isentropic turbulence. This may be related to the fact that even though that the experiment clearly shows anisotropic turbulence, the magnitudes of the normal stresses are in the same order. Considering the 'blind' results, the SST model runs in the k-ε mode ($F_1=0$) once the jet flow has left the injection line, while only at the vessel wall boundary layers there is a k-ω regime. This finding leads to the expectation that both simulations should provide quite similar results for the erosion process. Nevertheless, based on the velocity profiles a visibly stronger entrainment, i.e. a broader jet profile, is identified. The TKE level and profile is nearly comparable for both simulations, indicating that the dominant part of the TKE is produced inside the shear layers of the jet and thus the definition of the inlet turbulence level plays only a reduced role downstream near the tube exit.

Once the transition region of the initial density gradient is completely mixed, the transient progresses into a linear behavior. The FOV (PosB) of the PIV sequence around *t=1213 s* points onto the erosion front, i.e. the stagnation point of the jet slightly above the upper edge of the FOV (see Figure 8). At this time point, the damping effect of the helium layer is more significant, and the horizontal profiles are extracted in the upper third of the FOV. Qualitatively, the simulated and measured flow fields are in good agreement, while the quantitative assessment by means of the profiles identifies, consistent to the previous time point, showed a slightly broader jet.

Close to its stagnation point, the jet flow is redirected and the local anisotropy of the turbulent in the experiment becomes more pronounced but still remains in the same order of magnitude. Qualitatively, the

general characteristic of the TKE field is predicted by the model, while the magnitude in the jet axis is over predicted by roughly 20%.

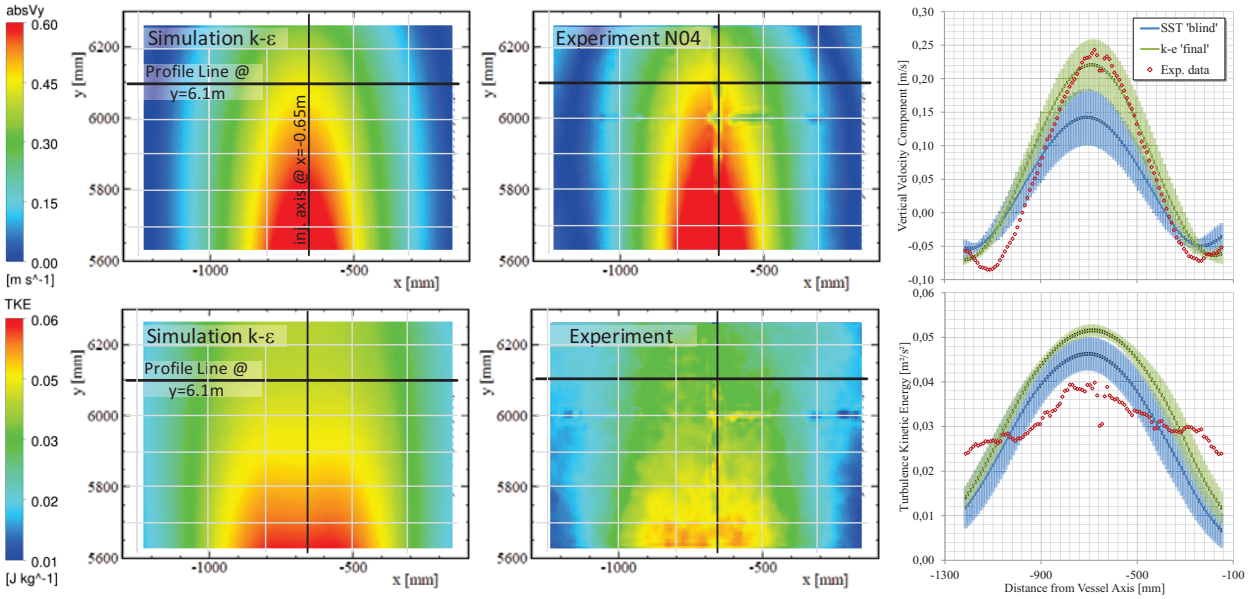

Figure 8: Comparison of averaged fields of the vertical velocity (left) and turbulence kinetic energy (middle) and extracted horizontal profiles (right) at t=1213 s (averaging interval: 204s)

The shape of the predicted TKE profile shows a strong radial decay of the TKE, while the experiment profile is visibly flatter due to the dominant horizontal fluctuations in vicinity of the stagnation point. Again, a visible deviation among the SST and k-ε results can be identified.

Following the erosion process, the FOV is moved further upwards to PosC. The PIV sequence around *t=1795 s* again shows that the erosion front and the stagnation point of the jet are clearly visible. Consistent with Figure 6, the jet stagnation point is predicted *~50 mm* above the measured one at *y~6750 mm*.

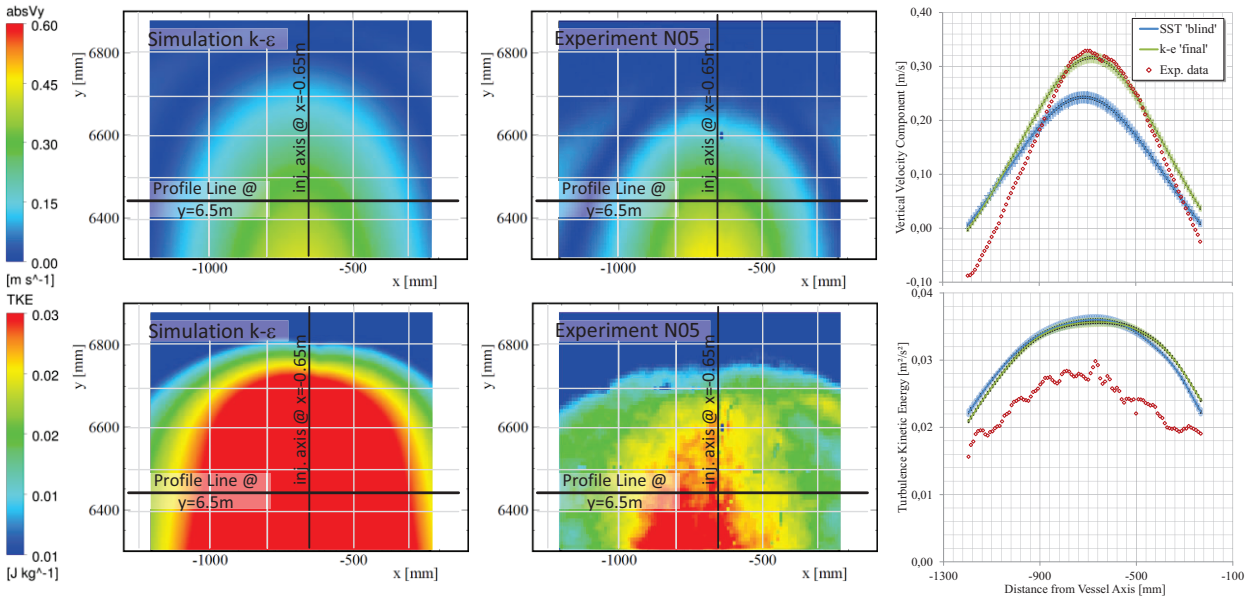

Figure 9: Comparison of averaged fields of the vertical velocity (left) and turbulence kinetic energy (middle) and extracted horizontal profiles (right) at t=1795 s (averaging interval: 204s)

Qualitatively, the result is in line with the previous time point. The predicted velocity magnitudes are quite comparable and a wider jet flow can be observed, e.g. by comparing the zero-velocity band in the 2D fields.

The TKE magnitude is over predicted by around *20%*. Nevertheless, one has to keep in mind that considering the TKE maximum of *~1.0 m²/s²* in the developing shear layer downstream, the tube exit is already at a very low level. Similar to the previous time point the measured TKE field shows a 'mushroom like' contour due to the horizontal fluctuations near the stagnation point which are not considered in the isentropic model.

Finally, the comparison against the PIV shows a consistent and improved prediction of the basic characteristics of the flow field close to the erosion front for the 'final' k-ε based model both from a qualitative and quantitative viewpoint. The remaining deviation is rated as acceptable. The difference in the predicted flow fields between the 'blind' SST model and the 'final' k-ε based model is remarkable and not expected, because the SST model runs in the k-ε mode once the jet has left the tube. For both simulations, it was verified that the jet flow is nearly symmetric to the measurement (x-y)-plane and not oscillating in the z-direction. Thus, an impact on the evaluated 2D fields can be excluded. The predicted TKE level at the erosion front is quite comparable for both models so that the small difference in the transient progression is correlated to the deviation in the flow field, i.e. the sharper jet predicted by the 'final' model results in a slightly faster mixing.

For the global mixing process, one has to consider the jet momentum $\rho \cdot \bar{v}$ arriving at the stratified layer. Consequently, it has to be proven that, in addition to the flow field, the density ρ of the jet arriving at the layer is consistent with the experiment. In the present case, radial heat and helium transfer with the ambient gas affect the jet core density. Figure 10 (left) gives a comparison of vertical density profiles along the jet axis and local measurements by means of gas compositions and temperatures. It must be noted that the measurements have been interpolated linearly in their sampling intervals of $\Delta t \leq 120\ s$ in order to provide a value at any given time point. In the early phase of the scenario, the jet density is increased due to the entrainment of cold air. Following the transient, the gas surrounding the jet is continuously enriched with helium coming from the mixing zone. Thus, this effect is reduced and after *~1500 s* the entrainment of helium rich gas leads to a slight decrease of jet density. These effects are well captured by the model while the maximum deviation of less than *5 %* occurs at the elevation of *y=5000 mm*. It is proven that the density in the mixing zone, characterized by a bend in the simulated density profile, is in very good agreement.

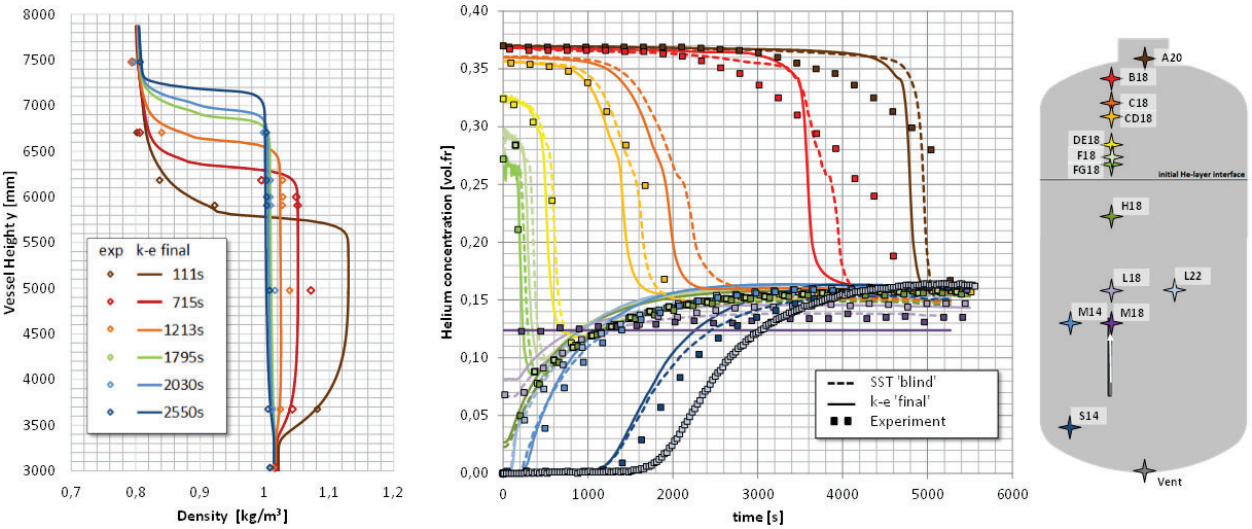

Figure 10: Comparison of the density profiles along the jet axis (left) and transient evolution of the pointwise concentration measurements during the transient for the blind SST and final k-ε simulation results (right)

Based on the consistent representation of the jet momentum and the turbulent kinetic energy in the mixing zone, the resulting helium transport and mixing process were investigated. Figure 10 (right) summarizes the comparison of the pointwise helium concentration measurements against the local concentration predicted by both models. On basis of the erosion front progression (Figure 6) it is already clear that the global transient progression is similar for both models. Taking into account the sensors FG18 up to C18

inside the layer one can observe that the temporal gradients are comparable and the drop in the concentration evolution, marking the erosion front, occurs slightly earlier for the 'final' simulation. Once the erosion front enters the upper torrospherical head of the facility (*t>2500s*) the sensors B18 and A20 histories show a visibly slower decrease in concentration which is not reproduced by both simulations. This indicates a deceleration of the erosion process in the test while instead both models predict a sudden drop. In the context of the general model validation, the focus is on the quasi-linear erosion process in the cylindrical part of the vessel where most of the measurements are located and the PIV data is available. There is no indication from the experiment, which explains the deviation observed once the erosion front enters the vessel dome. Consequently, this deviation is considered of less importance for the assessment of the model validity and may be resolved later.

Considering the transport and mixing of helium below the erosion front, measured e.g. at the sensor positions S14 to H18, one can identify a consistent increase of the local concentrations in time, indicating a reliable prediction of the helium transport.

Based on the systematic comparison of the experimental and simulated transient, a successful validation of the k-ε model based on measured as well as derived variables is concluded. The deviation between the SST model and the k-ε model is remarkable and needs further clarification.

5. SUMMARY

A systematic validation of a CFD approach aiming at the prediction of hydrogen transport and mixing hydrogen inside the containment building and connected compartments was carried out based on the OECD/NEA PANDA Benchmark test. The measurement data contains, in addition to the classical pointwise concentration measurements, 2D velocity measurements gained with PIV, which allow for a detailed validation of the underlying flow driving the erosion process. The dense data set allows not only for a direct comparison of measured values but also for an analysis of derived quantities. The validation methodology aimed at separating different error sources and thus avoiding a possible elimination of errors. It has been identified that e.g. the mesh resolution in the jet and mixing zone has only a minor impact, while small changes in turbulence modeling strategy or the chosen model constants, like Sc_t, significantly affect the simulation results. In particular, the comparison between the blind benchmark contribution based on the SST model and the open analysis employing the standard k-ε model highlights a remarkable effect of the selection of the turbulence model even though the SST model is running mostly in the k-ε mode. Based on this single validation case a general recommendation on the selection of the turbulence model or its suitability for this type of flow cannot be derived. However, this aspects needs to be analyzed carefully on further similar cases.

6. ACKNOWLEDGMENTS

The development of CFD models for prediction of H_2 mixing and mitigation were funded by the German Federal Ministry of Economic Affairs and Energy (Project No. 1501407) and performed in close cooperation with RWTH Aachen University.

7. REFERENCES

1. B. Smith "Assessment of CFD for nuclear reactor safety" *Proc. OECD/NEA and IAEA Workshop on Experiments and CFD Codes Application to Nuclear Reactor Safety (CFD4NRS-2)*, *NEA/CSNI/R(2009)12,* Grenoble, France, September 10-12 2008
2. M. Andreani, A. Badillo, R. Kapulla, "Synthesis of the OECD/NEA-PSI CFD Benchmark Exercise", *Proc. OECD/NEA and IAEA Workshop on Experiments and CFD Codes Application to Nuclear Reactor Safety (CFD4NRS-5)*, Zurich, Switzerland, September 9-11 2014

3. R. Kapulla, G. Mignot, S. Paranjape, D. Paladino, "Stably Stratified Helium Layer Erosion by a Vertical Buoyant Helium-Air Jet", *Proc. OECD/NEA and IAEA Workshop on Experiments and CFD Codes Application to Nuclear Reactor Safety (CFD4NRS-5)*, Zurich, Switzerland, September 9-11 2014
4. ANSYS, Inc., "ANSYS CFX-Solver Theory Guide and Solver Modeling Guide", Release 15, Canonsburg, October 2013
5. S. Kelm, M. Ritterath, H.-M. Prasser, H.-J. Allelein, "Application of the MiniPanda Test Case 'Erosion of a Stratified Layer by a Vertical Jet' for CFD Validation", *Proc. OECD/NEA and IAEA Workshop on Experiments and CFD Codes Application to Nuclear Reactor Safety (CFD4NRS-5)*, Daejeon, Korea, September 9-13 2012
6. R. Kapulla et al., "Break-up Of Gas Stratification in LWR Containment Induced by Negatively Buoyant Jets and Plumes", *Proc. ICONE-17*, Brussels, Belgium, July 12-16, 2009
7. M. Freitag, E. Schmidt, "Comparison Report for Blind and Open Simulations of THAI Test TH26 - Dissolution of a light gas stratification by air jet injection", Becker Technologies, *Project Report 1501455– TH26 – VB*, June 2014
8. E. Studer, et al: "Interaction of a light gas stratified layer with an air jet coming from below: Large scale experiments and scaling issues", *Nuclear Engineering and Design* **253**, 406– 412 (2012)
9. R. Kapulla, S. Kelm, G. Mignot, S. Paranjape, D. Paladino, "Experimental and Numerical Results for the Erosion Dynamics of a Vertical Helium-Air Jet interacting with a Helium Rich Layer", *Proc. International Congress on Advances in Nuclear Power Plants (ICAPP 2015)*, Nice, France, May 3-6 2015
10. OECD/NEA─PSI CFD Benchmark Specifications, final version, August 28th 2013
11. S. Kelm, J. Lehmkuhl, W. Jahn, H.-J. Allelein, "A Comparative Assessment of different Experiments on Buoyancy Driven Mixing Processes by means of CFD", *Proc. European Review Meeting on Severe Accident Research (ERMSAR)*, Marseille, France, March 24-26 2015
12. S. Kelm, W. Jahn, A. Schulze, H.-J. Allelein, "Passive auto-catalytic recombiner operation - validation of a CFD approach against OECD-THAI HR2-test", *Proc. OECD/NEA and IAEA Workshop on Experiments and CFD Codes Application to Nuclear Reactor Safety (CFD4NRS-4)*, Zurich, Switzerland, September 9-11 2014
13. F.R. Menter, et al. "CFD Best Practice Guidelines for CFD Code Validation for Reactor Safety Applications", EU-ECORA Project, EC Contract No FIKS-CT-2001-00154, 2001
14. M. Casey, T. Wintergerste, "ERCOFTAC Special Interest group on Quality and Trust in Industrial CFD – Best Practice Guidelines", ERCOFTAC (2000)
15. J. Mahaffy, et al., "Best Practice Guidelines for the use of CFD in Nuclear Reactor Safety Applications", *NEA/CSNI/R(2007)5*, 2007
16. Verein Deutsche Ingenieure, *VDI Waermeatlas*, 10th edition, Springer, 2006